NASA/TM—2017–219686

A Novel Solid State Ultracapacitor

A.Y. Cortés-Peña
Johnson Space Center, Houston, Texas

T.D. Rolin and S.M. Strickland
Marshall Space Flight Center, Huntsville, Alabama

C.W. Hill
CK Technologies, Meridianville, Alabama

August 2017

The NASA STI Program…in Profile

Since its founding, NASA has been dedicated to the advancement of aeronautics and space science. The NASA Scientific and Technical Information (STI) Program Office plays a key part in helping NASA maintain this important role.

The NASA STI Program Office is operated by Langley Research Center, the lead center for NASA's scientific and technical information. The NASA STI Program Office provides access to the NASA STI Database, the largest collection of aeronautical and space science STI in the world. The Program Office is also NASA's institutional mechanism for disseminating the results of its research and development activities. These results are published by NASA in the NASA STI Report Series, which includes the following report types:

- TECHNICAL PUBLICATION. Reports of completed research or a major significant phase of research that present the results of NASA programs and include extensive data or theoretical analysis. Includes compilations of significant scientific and technical data and information deemed to be of continuing reference value. NASA's counterpart of peer-reviewed formal professional papers but has less stringent limitations on manuscript length and extent of graphic presentations.

- TECHNICAL MEMORANDUM. Scientific and technical findings that are preliminary or of specialized interest, e.g., quick release reports, working papers, and bibliographies that contain minimal annotation. Does not contain extensive analysis.

- CONTRACTOR REPORT. Scientific and technical findings by NASA-sponsored contractors and grantees.

- CONFERENCE PUBLICATION. Collected papers from scientific and technical conferences, symposia, seminars, or other meetings sponsored or cosponsored by NASA.

- SPECIAL PUBLICATION. Scientific, technical, or historical information from NASA programs, projects, and mission, often concerned with subjects having substantial public interest.

- TECHNICAL TRANSLATION. English-language translations of foreign scientific and technical material pertinent to NASA's mission.

Specialized services that complement the STI Program Office's diverse offerings include creating custom thesauri, building customized databases, organizing and publishing research results…even providing videos.

For more information about the NASA STI Program Office, see the following:

- Access the NASA STI program home page at <http://www.sti.nasa.gov>

- E-mail your question via the Internet to <help@sti.nasa.gov>

- Phone the NASA STI Help Desk at 757–864–9658

- Write to:
  NASA STI Information Desk
  Mail Stop 148
  NASA Langley Research Center
  Hampton, VA 23681–2199, USA

NASA/TM—2017–219686

A Novel Solid State Ultracapacitor

A.Y. Cortés-Peña
Johnson Space Center, Houston, Texas

T.D. Rolin and S.M. Strickland
Marshall Space Flight Center, Huntsville, Alabama

C.W. Hill
CK Technologies, Meridianville, Alabama

National Aeronautics and
Space Administration

Marshall Space Flight Center • Huntsville, Alabama 35812

August 2017

Acknowledgments

A.Y. Cortés-Peña thanks Terry D. Rolin for his invaluable guidance and insight into this project as her mentor. She also thanks NASA's Motivating Undergraduates in Science Technology Program and the Hispanic Scholarship Fund for making her internship possible. She also thanks Mark Strickland, Patrick Mcmanus, Curtis Hill, Kathy Pressnell, Lee Allen, David Geist, Furman Thompson, Ron Hodge, Angela Shields, Angie Thoren, and staff in ES43 for supporting her project. This work has been paid in part by the Electrical, Electronic, and Electromechanical Parts, Packaging, and Fabrication Branch (ES43), the Center Innovation Fund, several NASA Marshall Space Flight Center Project Offices and has been funded by the NASA Georgia Space Grant.

Available from:

NASA STI Information Desk
Mail Stop 148
NASA Langley Research Center
Hampton, VA 23681–2199, USA
757–864–9658

This report is also available in electronic form at
<http://www.sti.nasa.gov>

TABLE OF CONTENTS

LIST OF FIGURES

LIST OF FIGURES (Continued)

LIST OF TABLES

LIST OF ACRONYMS, SYMBOLS, AND ABBREVIATIONS

AC	alternating current
AgZn	silver zinc
Al_2O_3	alumina
ALD	atomic layer deposition
$BaTiO_3$	barium titanate
DC	direct current
DF	dissipation factor
EEE	electrical, electronic, and electromechanical
EDLC	electrochemical double-layer capacitor
ESR	equivalent series resistance
H_2	hydrogen gas
HESSCap	high energy solid state capacitor
IBLC	internal barrier layer capacitor
LCR	inductance, capacitance, resistance
Li-ion	lithium-ion
N_2	nitrogen gas
O	oxygen
PdAg	palladium silver
SEM	scanning electron microscopy

Si	silicon
SiO_2	silica
SPS	spark plasma sintering
Ti	titanium

NOMENCLATURE

A	surface area
C	capacitance
D	distance
E	energy
e	electron
f	frequency
I	current
j	imaginary part of impedance
P	power
$P_{\max}$	maximum power
Q	stored charge
R	resistance, resistor
t	time
$\tan \delta$	loss tangent delta
V	voltage
V_f	final voltage
V_i	initial voltage
X	reactance
Z	impedance

NOMENCLATURE (Continued)

ε_0	vacuum permittivity
ε_{eff}	effective permittivity
ε_r	relative permittivity

TECHNICAL MEMORANDUM

A NOVEL SOLID STATE ULTRACAPACITOR

1. INTRODUCTION

NASA analyzes, tests, packages, and fabricates electrical, electronic, and electromechanical (EEE) parts used in space vehicles. One area that NASA wishes to advance is energy storage and delivery. Currently, space vehicles use rechargeable batteries that utilize silver zinc (AgZn) or lithium ion (Li-ion) electrochemical processes. These current state-of-the-art rechargeable batteries cannot be rapidly charged, contain harmful chemicals, and suffer from early wear-out mechanisms. A solid state ultracapacitor is an EEE part that offers significant advantages over current electrochemical and electrolytic devices. The objective of this research is to develop an internal barrier layer capacitor (IBLC) using novel dielectric materials as a battery replacement with a focus on such advantages as longer life, lower mass-to-weight ratio, rapid charging, on-demand pulse power, improved on-pad standby time without maintenance, and environmental friendliness.

Ultracapacitor behavior has been reported in a number of oxides including reduced barium titanate ($BaTiO_3$) ferroelectric ceramics. $BaTiO_3$ is a ceramic material in the perovskite family that possesses a high dielectric constant. Individual coating of ferroelectric $BaTiO_3$ grains with a silica (SiO_2) shell followed by spark plasma sintering (SPS) in reducing conditions has been shown to lead to stable ultracapacitor behavior. The permittivity values have been reported to be $\approx 10^5$ in electroceramics.[1] It has also been shown that treating oxidized $BaTiO_3$ at high temperatures in reducing forming gas atmosphere (96% nitrogen gas (N_2), 4% hydrogen gas (H_2)) produces an N-type semiconducting material.[2] The outer coating, which remains an insulating shell, combines with this semiconducting internal layer, resulting in millions of nanocapacitors in parallel. The combination of a semiconducting grain with an insulating boundary leads to the IBLC effect.

These so-called giant ultracapacitor properties are not easily controlled. The American Piezo Ceramics International reports a relative dielectric constant of 1,550 and a dielectric dissipation factor (DF) of 0.5 for single crystal $BaTiO_3$.[3] High permittivity values such as relative permittivity $\varepsilon_r \approx 10{,}000$ are reported in polycrystalline ferroelectric $BaTiO_3$. Reduced $BaTiO_3$ of grain sizes between 70 and 300 nm have yielded colossal permittivity values in the order of 10^5.[4] The purpose of this study is to evaluate shell-coated $BaTiO_3$ processed under reducing conditions to produce the IBLC effect.

2. BACKGROUND

2.1 Conventional Capacitors

A capacitor is an electrical component consisting of two conducting electrodes separated by an insulating dielectric material. When voltage is applied across the capacitor, opposite charges accumulate on the surface of each electrode, developing a static electric field. This field causes atoms in the insulator to polarize, producing an internal electric field. Capacitors are able to store energy in this overall electric field. This is illustrated in figure 1.

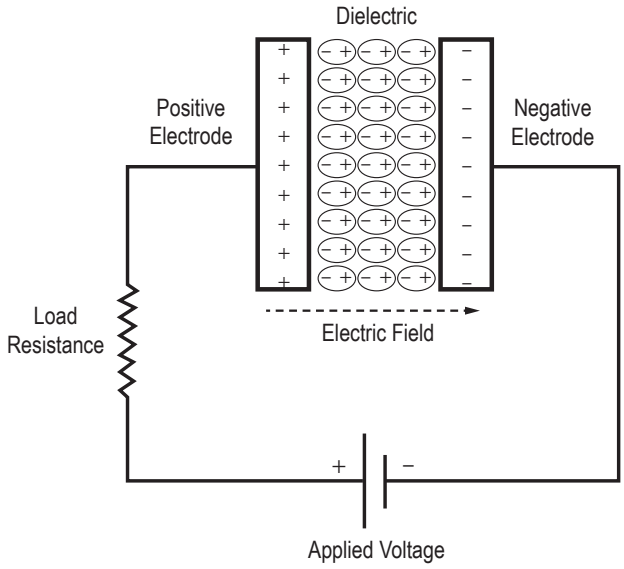

Figure 1. Schematic of a conventional capacitor.[5]

Capacitance is a measure of the ability to store charge, and it is the ratio of the stored charge Q to the applied voltage V:

$$C = \frac{Q}{V} \quad . \tag{1}$$

The capacitance can be improved by increasing the electrode surface area A and decreasing the distance between the plates. It is also proportional to the ε_r, which measures how much electric flux is generated per unit charge, and it is directly related to how easily a specific material polarizes in response to an electric field. The vacuum permittivity ε_0 is a constant due to free space vacuum and

is 8.854187…× 10^{-12} F/m. The relative permittivity multiplied by the vacuum permittivity is usually called the effective permittivity ε_{eff}:

$$C = \varepsilon_0 \varepsilon_r \frac{A}{D} \quad . \tag{2}$$

Capacitive loads oppose the change of voltage. Impedance Z is a measure of the effect of capacitive loads. When reactance X is zero, the load is purely resistive; when resistance R is zero, the load is purely reactive. Ideal capacitors consist entirely of reactance, having infinite resistance:

$$Z = R + jX \tag{3}$$

and

$$X_C = \frac{1}{2\pi f C} \quad . \tag{4}$$

Loads are modeled as either series or parallel combination of a resistive and a reactive load. The parallel resistance is typically larger than the series resistance. To measure small reactive values, such as high-valued capacitors, it is preferable to use the series model because the series resistance is more significant than the parallel resistance. When measuring large reactive values, such as high-valued inductors or low-valued capacitors, it is preferable to use the parallel model. Table 1 shows the capacitance ranges and which model should be used.[6]

Table 1. Model for corresponding capacitance ranges.

Range	Impedance (Ω)	Model
>100 µF	<10	Series
10 nF – 100 µF	10 – 10,000	Series or parallel
<10 nF	10,000	Parallel

At low frequencies, a capacitor is an open circuit, as no current flows in the dielectric. A direct current (DC) voltage applied across a capacitor causes positive charge to accumulate on one side and negative charge to accumulate on the other side; due to the accumulated charge, the electric field is the source of the opposition to the current. When the potential associated with the charge exactly balances the applied voltage, the current goes to zero. Driven by an alternating current (AC) supply, a capacitor will only accumulate a limited amount of charge before the potential difference changes polarity and the charge dissipates. The higher the frequency, the less charge will accumulate and the smaller the opposition to the current.[7]

The two primary attributes of a capacitor for this study are its energy density and power density. The energy E stored in a capacitor is directly proportional to its capacitance:

$$E = \frac{1}{2} C V^2 \quad . \tag{5}$$

To determine power, capacitors are represented in series with an external load resistance R, shown in figure 1. The internal components of the capacitor itself contribute to the resistance as the equivalent series resistance (ESR). Maximum power $P_{\max}$ for a capacitor occurs at matched impedance (R=ESR)[8]:

$$P_{\max} = \frac{V^2}{4 \times \mathrm{ESR}} \quad . \tag{6}$$

ESR is an AC resistance dependent on frequency. In nonelectrolytic capacitors, such as electroceramics, the resistance of the leads and electrodes and losses in the dielectric cause the ESR. For a capacitor, the ESR typically falls between 0.001 and 0.1 Ω and is desired to be low.[9] A high ESR represents increased heat dissipation, and results in accelerated aging under high temperature and large ripple current conditions. Additionally, capacitors exhibiting high ESR have a high current leakage, consuming and wasting power in the idle state, making them bad energy storage devices[10]:

$$P = I^2 \times \mathrm{ESR} \quad . \tag{7}$$

Electrical potential energy is dissipated in dielectric materials in the form of heat. The DF is a measure of loss-rate of energy and is proportional to the ESR. The DF is also known as loss tangent delta, tan δ, and it is represented as a percentage. This parameter depends on the dielectric material and the frequency of the electrical signals. In high dielectric constant ceramics, DF can be 1%–2%[11]:

$$\tan\delta = \frac{\mathrm{ESR}}{|X_C|} = \mathrm{DF} \quad . \tag{8}$$

Dielectric tan δ of ceramic capacitors is dependent upon specific characteristics of the dielectric formulation, level of impurities, as well as microstructural factors such as grain size, morphology, and porosity (density).[10]

2.2 Electrochemical Double-Layer Capacitor

Conventional capacitors have relatively high-power densities but low energy densities when compared to electrochemical batteries. Stated another way, a battery may store more energy but cannot deliver it as quickly as a capacitor can. Current ultracapacitors exploit high surface area electrodes and thin dielectrics to increase both capacitance and energy. Additionally, ultracapacitors have advantages over electrochemical batteries and fuel cells, including higher power density,

shorter charging times, and longer cycle life and shelf life.[5] The Ragone chart in figure 2 compares the power and energy densities of different types of current energy storage devices.

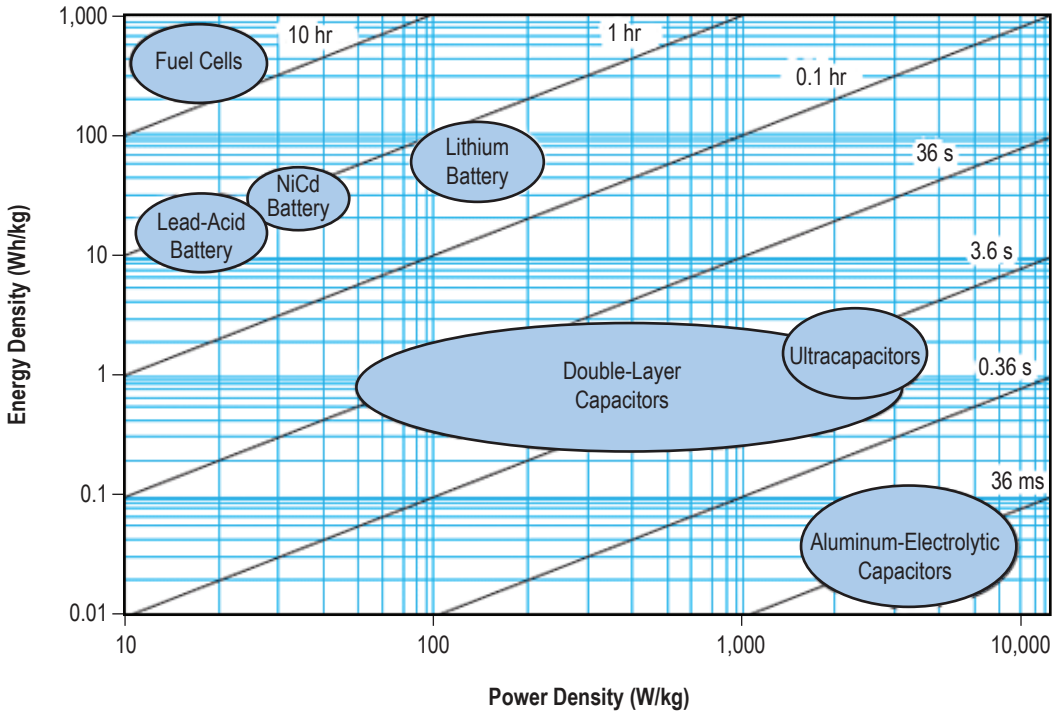

Figure 2. Ragone chart of energy storage devices. Source: Defense Logistics Agency Land and Maritime.

Electrical characteristics of ultracapacitors today lie between those of aluminum-electrolytic capacitors and fuel cells. The electrochemical double-layer capacitor (EDLC) (fig. 3) uses high surface area electrodes to elicit ultracapacitor behavior. EDLCs are constructed from two carbon-based electrodes, an electrolyte, and a separator. Ions within the electrolyte solution accumulate at the surface of the electrodes, and the separator creates a double-layer of charge.[12] EDLCs generally operate with stable performance characteristics for many charge/discharge cycles, sometimes as many as 10^6 cycles. On the other hand, electrochemical batteries are generally limited to only about 10^3 cycles.[5] Because of their cycling stability, EDLCs are well suited for applications that involve nonuser serviceable locations (e.g., deep sea and mountain environments). However, packaging paradigms for EDLCs do not permit their use in aerospace environments without hermetically sealed containers, which increase mass and volume. Currently, electrolytic ultracapacitors are used primarily in conjunction with batteries in terrestrial environments to capture sudden bursts of energy (e.g., regenerative braking systems). However, electrolytic ultracapacitors do not possess the energy density necessary to replace batteries.

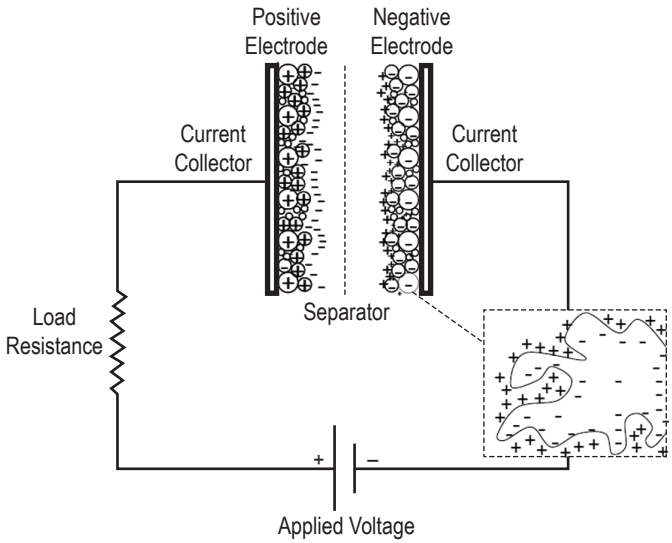

Figure 3. Schematic of an EDLC.[5]

2.3 Internal Barrier Layer Capacitor

A solid state ultracapacitor would overcome the limits of both the electrochemical batteries used on spacecraft and available electrochemical ultracapacitors. It provides a robust energy storage device with higher reliability and less weight and volume than electrochemical batteries and electrolytic ultracapacitors. Solid state ultracapacitors are recyclable energy storage devices that offer the promise of higher power and greater number of charge/discharge cycles than current rechargeable batteries, and they will also offer greater breakdown voltage than current electrolytic ultracapacitors. The presented research is for technology leading to a high-energy solid state capacitor (HESSCap) module to replace batteries and current state-of-the-art ultracapacitors. Table 2 presents the primary parameters for aerospace batteries and terrestrial electrolytic ultracapacitors and the target values for the HESSCap.

Table 2. Ultracapacitor/Battery comparison.

Device	Energy Density (J/cc)	Charge/Discharge Cycles	Voltage (V)
Aerospace battery (Li-ion)	172	500 – 2,000	28
Aerospace range safety battery (AgZn)	57	<12	28
Commercial electrolytic ultracapacitor	15	>500 w/ 50% V and 25% *C* decrease	59
ES43 solid state cell (28 V)	80 – 200	>500,000	28

The HESSCap module achieves high permittivity via the IBLC effect, shown in figure 4. Individual ferroelectric grains are coated by a dielectric shell followed by sintering at high temperatures and reducing forming gas atmosphere (96% N_2, 4% H_2). The forming gas penetrates the shell and reacts with the inner grain, making each grain semiconductive. The coating serves as an insulator, resulting in millions of nanocapacitors in parallel:

$$C_{\text{total}} = C_1 + C_2 + \ldots + C_n \quad . \tag{9}$$

The two main conditions for the internal barrier layer to increase the overall dielectric permittivity of oxides are the inner grain conductivity and the insulating grain boundary. The former is related to the amount of charged defects intentionally formed during the sintering step under reducing conditions.[4] The IBLC model can be applied to any material where extended dielectric interfaces of very small thickness separate (semi)conducting parts: in ceramics, insulating grain boundaries surround conducting grains; in thin films and multilayers, surfaces and intergrowth planes can induce dielectric barriers between conducting layers.[13] However, the exact nature of the conduction mechanism within the grains and of the charge accumulation at the grain boundaries is not well understood.

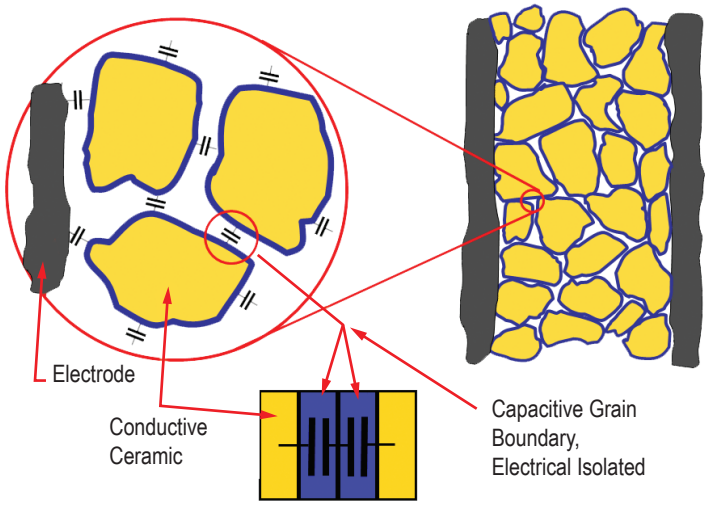

Figure 4. IBLC effect.

3. METHODOLOGY

3.1 Atomic Layer Deposition-Coated Ceramic Barium Titanate Nanoparticles

This study focuses on $BaTiO_3$ particles of various sizes in both coated and uncoated configurations, with the latter serving as a baseline. Table 3 provides the details on particle diameter, coating material and thickness, purity, and supplier.

Table 3. $BaTiO_3$ materials.

Supplier	Particle Size (nm)	Purity (%)	Coating	Thickness (nm)	Color
Ferro	730	99.95	Uncoated	–	White
TPL, Inc.	500	99.95	SiO_2	5	Light grey
ALD NanoSolutions	500	99.95	Alumina	10	White

The $BaTiO_3$ particles used in this study varied in median diameter, also known as particle size distribution D50, ranging from 500 to 730 nm. Coating configurations varied from uncoated to 10 nm. The uncoated $BaTiO_3$ sample was a fine powder, while the coated $BaTiO_3$ samples had agglomerated powder. The clumps are likely caused by hydrophilic interaction or static charge. The clumps were dispersed before processing using ink formulations.

Atomic layer deposition (ALD) was used to deposit nano-thin films over $BaTiO_3$ nanoparticles. ALD is based on the sequential use of a proprietary gas phase chemical process. The nano-thin film coatings consist of 10 nm alumina (Al_2O_3) and 5 nm SiO_2. Figure 5 shows a transmission electron microscope image of a coated $BaTiO_3$ particle used in this study. The number of cycles achieved during ALD determines the coating thickness. The coating thickness rate for Al_2O_3 was 10 Å per cycle and for SiO_2 was 4 Å per cycle. It is important to note that previous IBLC research using SPS of $BaTiO_3$ particles were coated by the Stöber process, a method based on a seeded growth process.[1,14] The Stöber process is known to produce an inconsistent coating.

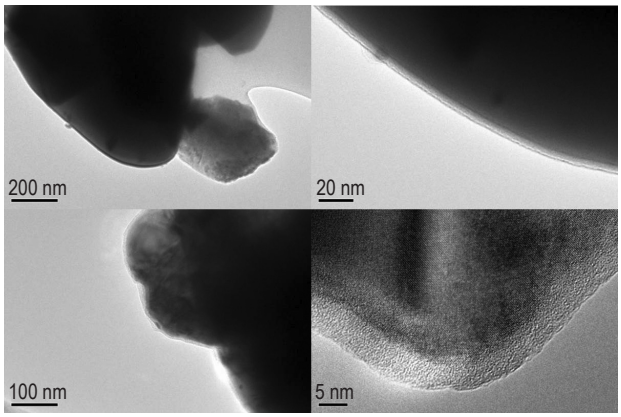

Figure 5. $BaTiO_3$ nanoparticle with 5 nm of SiO_2 coating.

SiO_2-coated $BaTiO_3$ becomes oxygen deficient and semiconductive under vacuum sintering condition, turning the coating layer into an isolating insulator layer.[1] It was thought that the structure became that of the internal barrier layer semiconductor ceramics. However, the location of SiO_2 determined by a silicon (Si) elemental mapping of disk cross section by scanning transmission electron microscopy-energy diversive spectroscopy (STEM-EDS) detects almost no Si elements in the grain boundary of $BaTiO_3$; instead, it is segregated. This implies that Si plays no important role of insulation because it cannot stay on the surface of grains. Rather, it diffuses during the sintering process.[15] Some testing performed at Auburn University suggests the opposite; namely, there does appear to be SiO_2 remaining on the surface grains. Whatever the interaction between semiconducting $BaTiO_3$ and its coating may be, the colossal permittivity values cannot be ignored, so this coating was kept under consideration for this investigation.

3.2 High-Temperature and Reduced Forming Gas Sintering

In reducing atmospheres (96% N_2, 4% H_2), $BaTiO_3$ is slightly reduced, forming doubly ionized oxygen (anion) vacancies. This produces the same effect as vacuum sintering, so a reducing atmosphere was the preferred method of processing. To understand vacancy creation, a $BaTiO_3$ crystal structure is shown in figure 6. The conductivity results from the electron exchange between Ti^{+4} and Ti^{+3} because oxygen vacancies are created at the octahedron.[2] The induced free electrons make the reduced perovskite material highly semiconducting. Sintering $BaTiO_3$-based dielectrics in forming gas decreases the insulation resistance (IR) by 10–12 orders of magnitude[16]:

$$BaTiO_3 + xH_2 \rightarrow = BaTiO_{3-x}\left[V_O\right]_x + xH_2O \tag{10}$$

and

$$\left[V_O\right] \rightarrow = \left[V_O\right]^{\cdot\cdot} + 2e \quad . \tag{11}$$

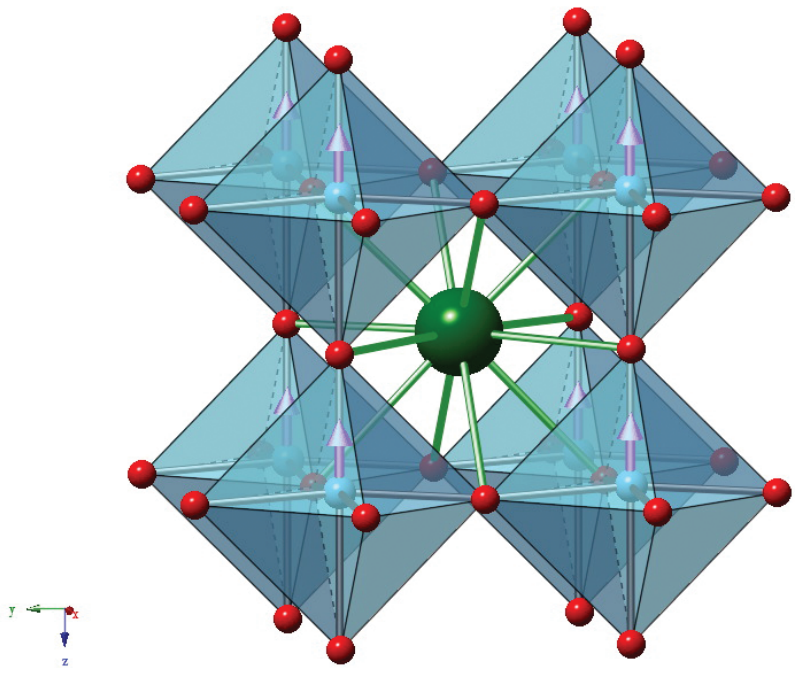

Figure 6. The $BaTiO_3$ crystal structure. The green, red, and blue atoms are titanium, oxygen, and barium, respectively. Source: <www.crystalmaker.com>.

A three-zone Thermo Scientific™ Lindberg Blue™ tube furnace was used to process the particles. The furnace was heated uniformly to 300 °C, left to hold for an hour to avoid thermal shock of the quartz tube, and then set to the desired temperature ranging from 500 °C to 1,100 °C. The duration varied from 1 to 30 hr. Three quartz boats were each filled with 5 g of Al_2O_3-coated, SiO_2-coated, and uncoated $BaTiO_3$. The uncoated $BaTiO_3$, serving as a baseline, was always heat treated to evaluate its electrical properties versus those of coated particles. The forming gas was turned on at 3 SCFH for 10 min prior to placing the samples inside. After the desired annealing duration, the furnace was set to cool to 300 °C with the forming gas flowing to avoid any reoxidation of the samples while exposed to high temperatures. The furnace was then opened and observations were made on the color of the samples inside the tube furnace. Finally, the forming gas was turned off and the samples were left to cool to room temperature inside the tube furnace before removal.

Previous studies show that the reduction of $BaTiO_3$ in H_2 at intermediate temperatures (500 °C) leads to bodies of bright yellow color.[17] Significantly reduced SiO_2-coated material obtained through SPS at a final temperature of 1,110 °C is expected to change from white to a navy blue color.[3] Uncoated $BaTiO_3$and doped $BaTiO_3$ specimens that show a remarkable reduction in resistivity have also been characterized with a bluish color.[18] To assess color changes, optical microscopy images of the pellets were taken at 7× magnification.

When powdered particles are heated to a high temperature below the melting point, the atoms in the powder diffuse across the particle boundaries fusing the particles together. Two additive manufacturing techniques used for electrode and dielectric deposition, such as aerosol jet

deposition and screen printing, require unfused particles in order to deposit the material properly. In order to screen print the particles, they were separated using a three-roll mill.

3.3 Pellet Electrical Characterization

The unsintered powders were pressed into pellets, without the addition of binder, using a potassium bromide die. A literature review revealed that pellets pressed at pressures above 50,000 psi could not be recovered.[19] Various pressures were tested revealing that pellets pressed at forces above 400 lb could not be recovered from the potassium bromide die in suitable shape. Because of these findings, the pellets were pressed at 300 lbf using a TestResources, Inc., compression and tension machine. The pellets were 4–8 mm thick with masses of 1.5–2.5 g.

The adsorption of water vapor increases the permittivity by a factor of two.[19] However, the focus of the characterization at this phase of the study was to identify a sample with a large change in permittivity, specifically by a factor of 10^4. Because the focus was large changes in permittivity, no attempt was made to remove the water. In addition, thin film electrical characterization is used to obtain the most accurate measurements, and since the thin films undergo sintering, the water absorption effects are eliminated.

Capacitance, DF, and ESR were measured for a frequency range of 20 Hz to 2 MHz using a Dielectric Test Fixture 1645-1B together with an Agilent E4980A precision inductance, capacitance, and resistance (LCR) meter, shown in figure 7. The capacitance was initially assumed small; therefore, measurements were made using the LCR meter's parallel model. If the values were found to be higher than expected, then the instrument could be reset to use a series model for accuracy. The dielectric constant of the samples was determined from the instrument's reported capacitance value. No porosity correction was made to the dielectric constant.

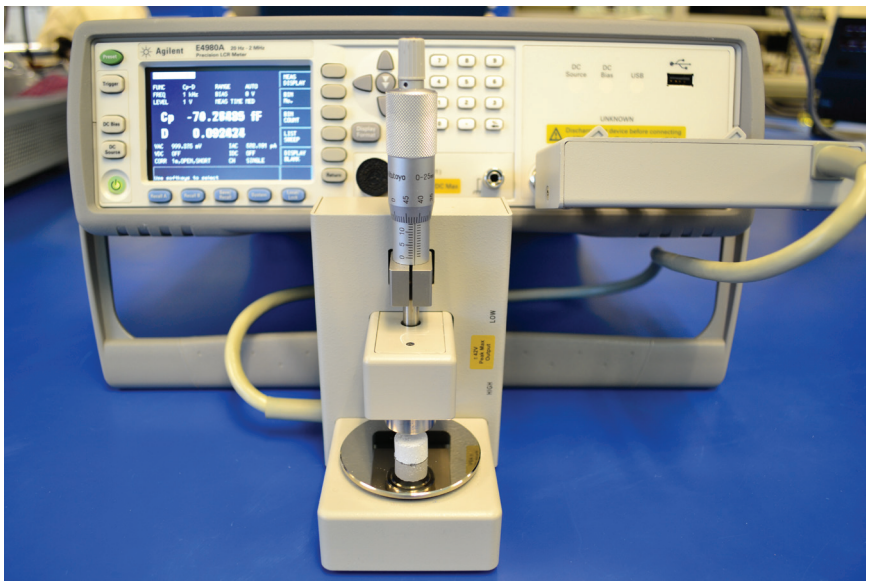

Figure 7. Dielectric Test Fixture 1645-1B (bottom) and Agilent E4980A precision LCR meter (top).

3.4 Dielectric Ink Formulation

To perform 3D additive manufacturing, the powders were first converted into an ink. The formulation for this ink is shown in table 4. Glass particulates were used to increase densification, but high quantities of glass particles decrease the permittivity, so the concentration of glass was kept as low as possible to produce a usable ink. Surfactant was used as a wetting agent to allow the ink to spread. A thinner was also used obtain the proper ink viscosity. Texanol was used as a thinner because it volatilizes at 120 °C. The vehicle was an organic binder formulated from a blend of Ashland Chemical Ethyl Cellulose N200 in Texanol, and it was used to further enhance the viscosity of the ink. The vehicle was chosen because it volatilizes between 250 °C and 350 °C during sintering.

Table 4. Dielectric ink formulation.

Component	Concentration (%)
$BaTiO_3$ dielectric	72.5
Lead-germinate high K glass	7.5
Surfactant (wetting agent)	0.5
Texanol (solvent)	5
Ethyl cellulose organic vehicle	15

The dielectric ink formulation was mixed and then ground in a three-roll mill. A three-roll mill is a tool that uses shear force from three horizontally positioned rolls rotating at opposite directions and different speeds relative to each other to mix, refine, disperse, and homogenize viscous materials fed into it. The final ink was a dense, homogenous mixture used for screen printing.

3.5 3D Additive Thick Film Deposition

The screen printing method was the chosen method of printing a test cell for this study. This technique can produce layers as thin as 5 μm. By producing such a thin dielectric layer, the capacitance relationship (eq. 2) shows that the energy stored can be increased significantly. The screen printing process began by creating a design on a woven mesh using photolithography. The ink was forced into the mesh openings by a squeegee and onto the printing surface during the squeegee stroke. The larger the number of intertwined meshes, the thinner the deposition becomes for a single stroke. The capacitor layers (fig. 8) were printed using a Hary Manufacturing, Inc. 485 precision screen printer. Palladium silver (PdAg) ink that is used in multilayer chip capacitors due to its conductance and resistance to silver migration was used as the electrode material. Al_2O_3 (0.039 in, 96% purity) was used as the substrate on which each layer was deposited. Al_2O_3 was chosen because it has a very low coefficient of expansion and will not impart excessive stress during later sintering steps. As a result, each layer is only able to densify in the axis perpendicular to the substrate, due to clampling to the substrate. The ultracapacitor test cells were made using two layers of dielectric applied through 325 and 400 mesh screens, respectively.

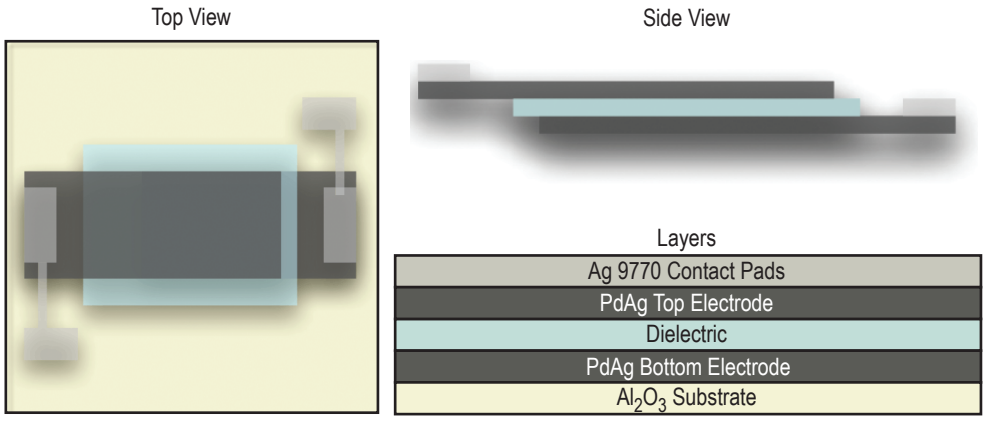

Figure 8. Top and side view of the ultracapacitor module layers.

The capacitor test cell was sintered, using an HSA1505-0811Z belt furnace from Hengli Eletek Company, at 850 °C peak for 10 min, and a total cycle time of 1.5 hr. This sintering step was performed after each layer deposition in order to burn off organic materials and achieve high densification. The temperature settings of the eight-zone belt furnace are shown in figure 9, the temperature profile in figure 10, and the nitrogen flow profile in table 5. Previous work shows that when reduced SiO_2-coated $BaTiO_3$ is post-annealed at 800 °C for 12 hr in air, it remains blue, while reduced uncoated $BaTiO_3$ turns white.[13] For this reason, the SiO_2 shell was thought to act as an efficient barrier against oxidation. As a further preventative measure, the belt muffle furnace was purged with nitrogen to avoid reoxidation. Densification of the dielectric layer was then evaluated with the scanning electron microscope (SEM).

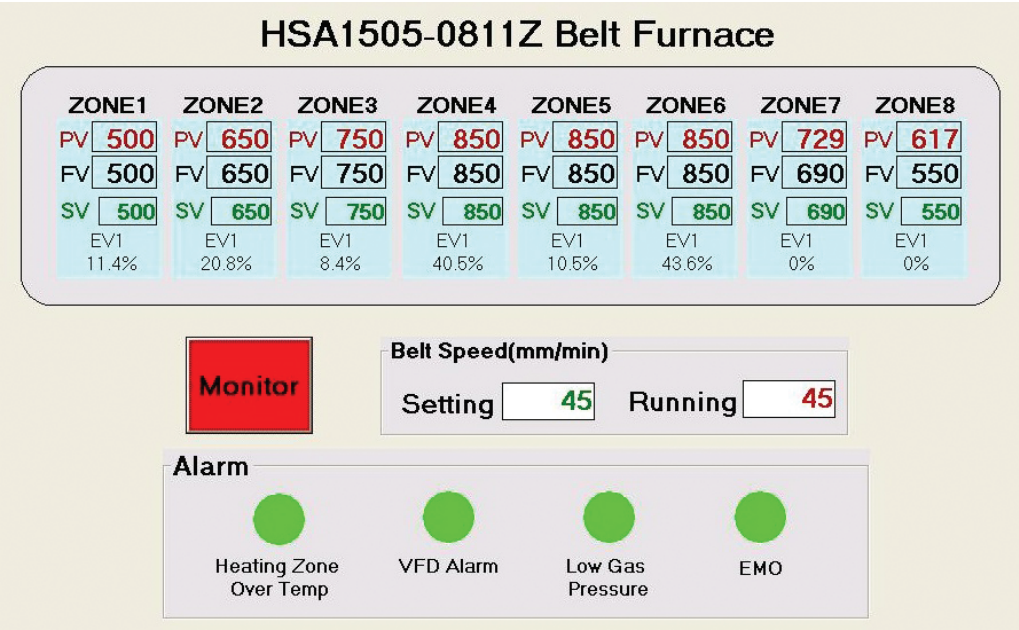

Figure 9. Eight-zone belt furnace temperature settings.

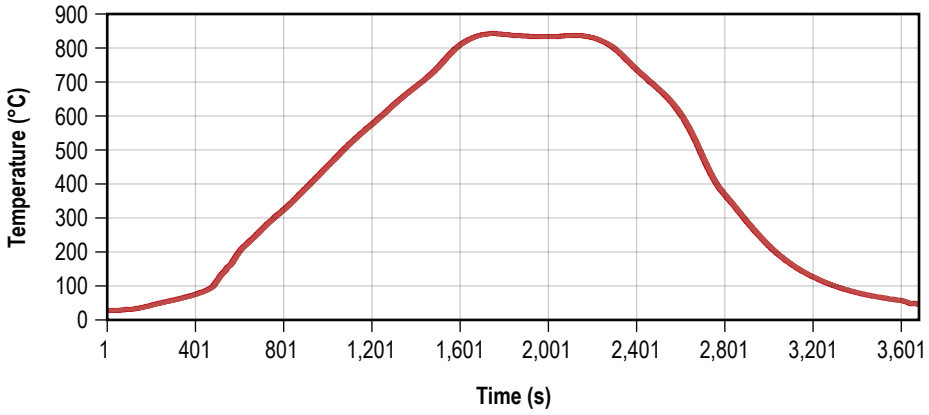

Figure 10. Belt furnace temperature profile.

Table 5. Furnace nitrogen flow profile.

Section	Nitrogen Flow (LPM)
Entrance curtains	40
Preheat	45
Venturi exhaust	100
Cooling gas	20
Exit curtains	20

3.6 Thick Film Electrical Characterization

The ultracapacitor test cell was measured for parallel capacitance using the LCR meter. Capacitance readings were then used to determine if the device was functional. When readings were found to be unstable, due to either shorted electrodes or low ESR values, the capacitance was measured using the discharge method. To use the discharge method, the capacitor was discharged through a resistor determined to yield a reasonable time constant. The voltage versus time plot was captured with a DPI5104 digital phosphor oscilloscope. A large region of the discharge curve was chosen, and the values of voltage in the discharge cycle and time required to drop between the two voltages were entered into equation (12) along with the known resistor value. In this equation, t is the time it takes to discharge the capacitor between some initial voltage V_i to some final voltage V_f: C is the capacitance to be determined, and R is a resistor through which the capacitor is discharged:

$$t = C \times R \times \ln\left(\frac{V_C}{V_i}\right) \quad . \tag{12}$$

4. ANALYSIS

4.1 Pellet Electrical Characterization

SEM images of the untreated powders (figs. 11(a) and (b)) revealed that particles indicated by the manufacturer to be 500 nm actually varied in diameter from 250 nm up to 1 μm. Treated powders (fig. 11(c)) also showed varying particle sizes of the same range. These observations showed that the furnace treatment was not causing grain growth.

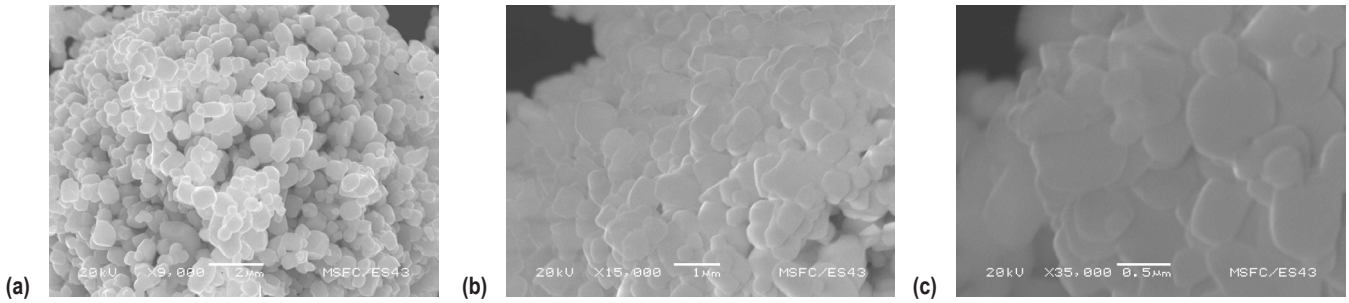

Figure 11. SEM images of $BaTiO_3$ (a) uncoated from TPL, (b) coated with Al_2O_3, and (c) Al_2O_3-coated treated at 750 °C for 30 hr.

All three configurations of powder batches were initially white in color, as can be seen in figure 12. When treated at temperatures below 900 °C, they turned to a bright yellow or neon green color. These powders remained that color under the reduced forming gas atmosphere and changed to white after the first minute of exposure to air. Scraping off the top layer of the treated powder revealed two shades of color, a lighter tone on top and a darker tone underneath. This nonuniform color, shown in figures 13 and 14, indicates that the particles were not being sintered homogeneously.

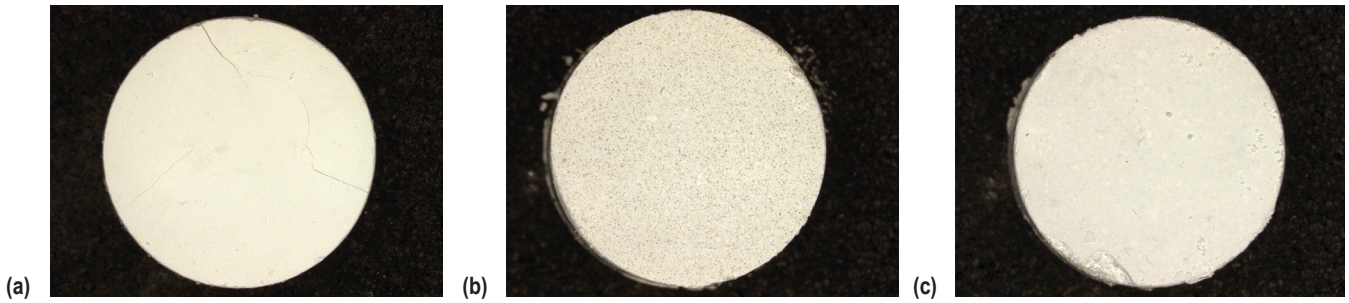

Figure 12. Optical microscopy photographs of untreated (a) uncoated, (b) SiO_2-coated, and (c) Al_2O_3-coated $BaTiO_3$ pellets.

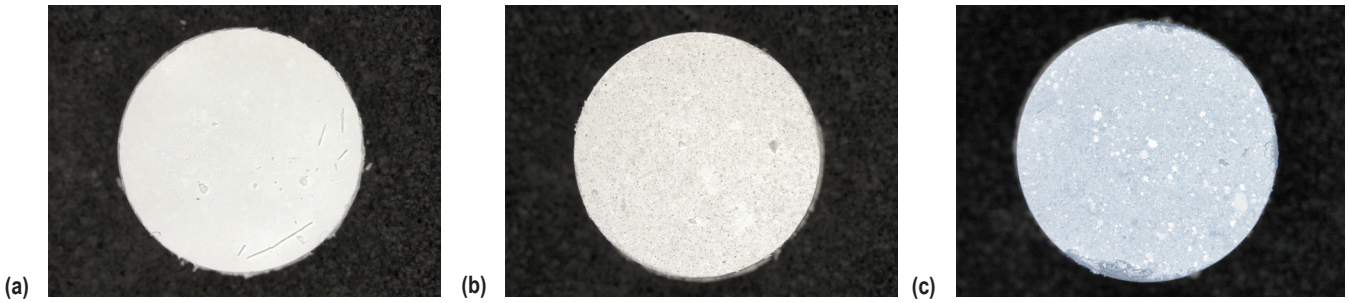

Figure 13. Optical microscopy photographs of (a) uncoated, (b) SiO_2-coated, and (c) Al_2O_3-coated $BaTiO_3$ pellets treated at 900 °C for 1 hr.

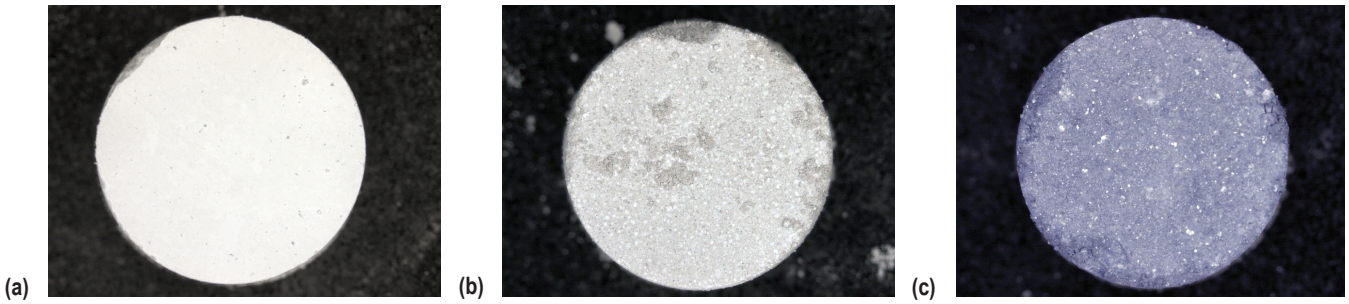

Figure 14. Optical microscopy photographs of (a) uncoated, (b) SiO_2-coated, and (c) Al_2O_3-coated $BaTiO_3$ pellets treated at 1,100 °C for 1 hr.

At temperatures below 900 °C, no significant changes are seen in the permittivity. At temperatures above 900 °C, the permittivity and DF slightly increased for uncoated $BaTiO_3$ and decreased for coated samples. The ESR decreased only for the Al_2O_3-coated sample, the greatest decrease occurring with 900 °C treatment. The decrease in ESR coincides with the color change (fig. 15) which can be interpreted as the material undergoing reduction.

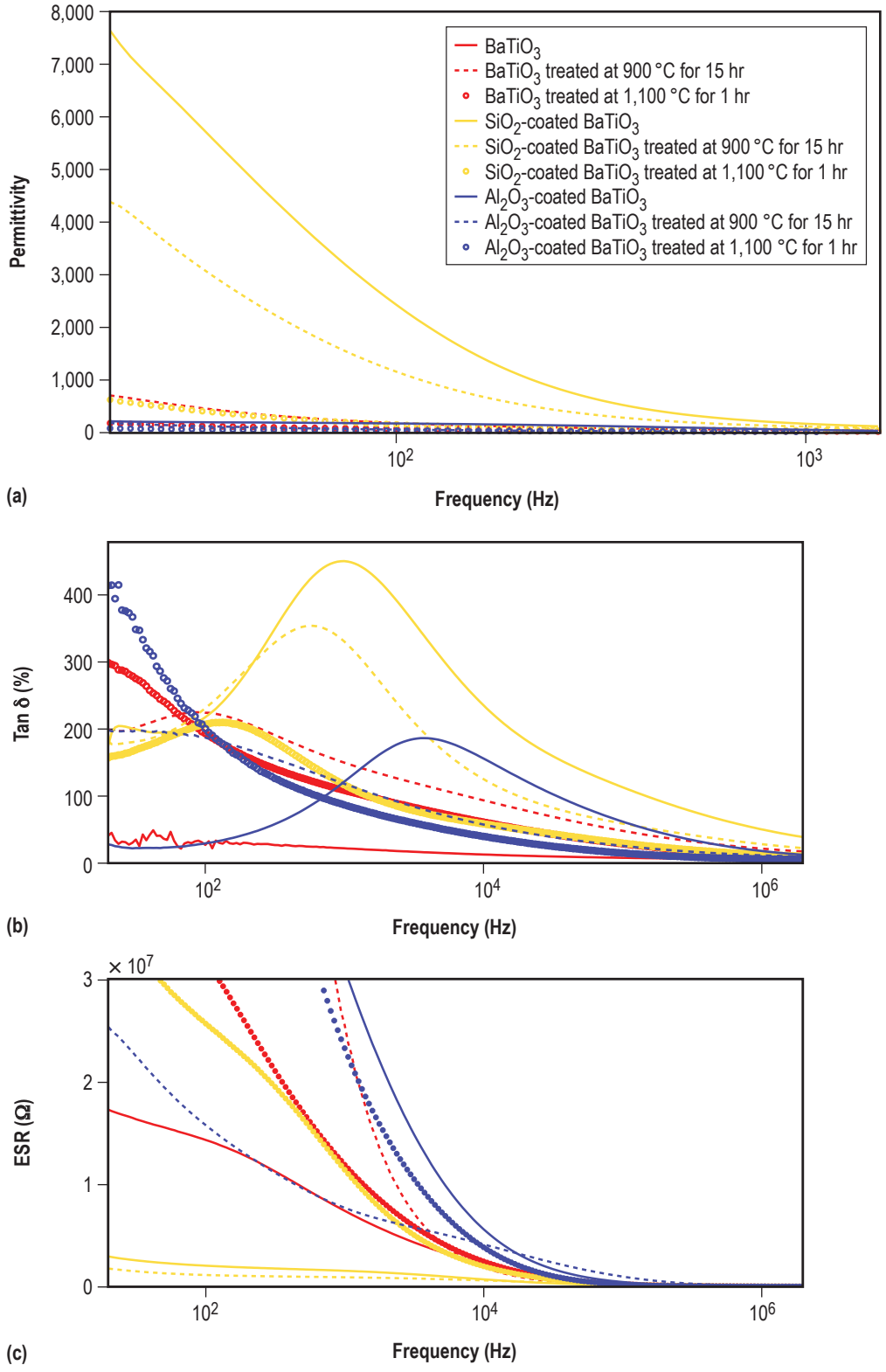

Figure 15. Plots of (a) permittivity, (b) DF, and (c) ESR samples treated at 900 °C for 15 hr and 1,100 °C for 1 hr compared to the untreated powders.

The synthesis profile that produced the maximum increase in permittivity for all samples was at 900 °C for 1 hr. Table 6 shows the effect of a short-duration treatment versus a long-duration treatment with constant (900 °C) temperature. The SiO_2-coated sample exhibits the highest permittivity.

Table 6. Synthesis profile effect on dielectric permittivity.

$BaTiO_3$ at 20 Hz	Untreated		1 Hour at 900 °C		15 Hours at 900 °C	
	Color	Permittivity	Color	Permittivity	Color	Permittivity
Uncoated	White	9	White	2,227	White	708
Al_2O_3-coated	White	217	Light blue	6,866	Navy blue	182
SiO_2-coated	White	7,638	Grey	19,980	Grey	4,384

The capacitor properties versus frequency of the samples treated at 900 °C for 1 hr are compared in figure 16. Low-frequency permittivities are high (maximum 19,980 at 20 Hz), indicating the dielectric may useful for DC applications. The DF was found to increase with treatment, and it is likely that further sintering will decrease the rate of energy loss. The decreased ESR for all treated powders indicates that they are becoming semiconducting, one of the desired outcomes for the IBLC effect. SiO_2-coated and Al_2O_3-coated $BaTiO_3$ treated at 900 °C for 1 hr were chosen as the dielectric for the capacitor test cell because of the best capacitance traits.

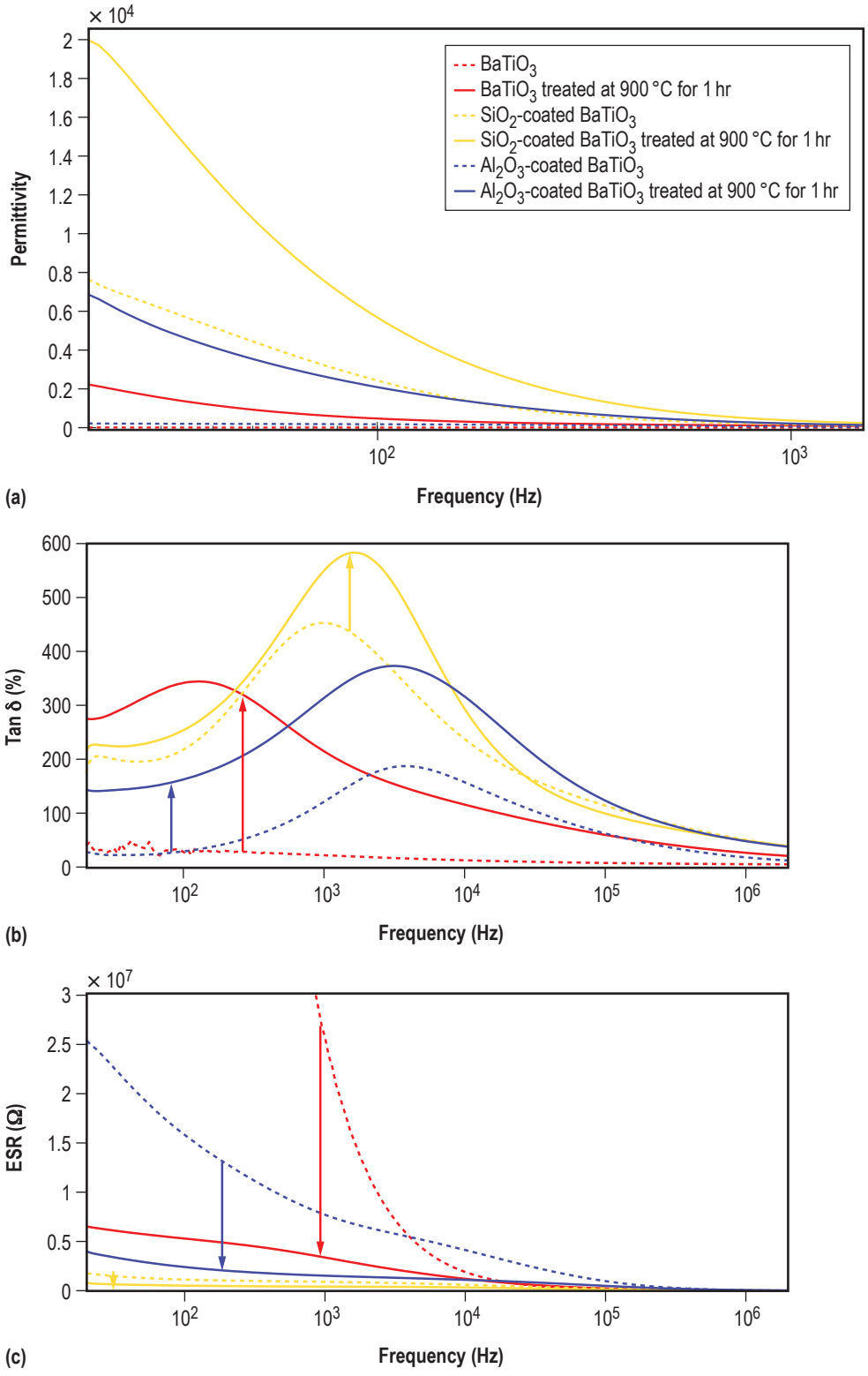

Figure 16. Plots of (a) permittivity, (b) DF, and (c) ESR samples treated at 900 °C for 1 hr compared to the untreated powders.

4.2 Thick Film Electrical Characterization

The color of the dielectric ink made up of Al_2O_3 and SiO_2 were initially light blue and grey, respectively. After deposition on the substrate followed by sintering, both changed color to snow white, a much whiter tone than observed in the untreated powders. Figure 17 shows an ultracapacitor test cell made with SiO_2-coated $BaTiO_3$.

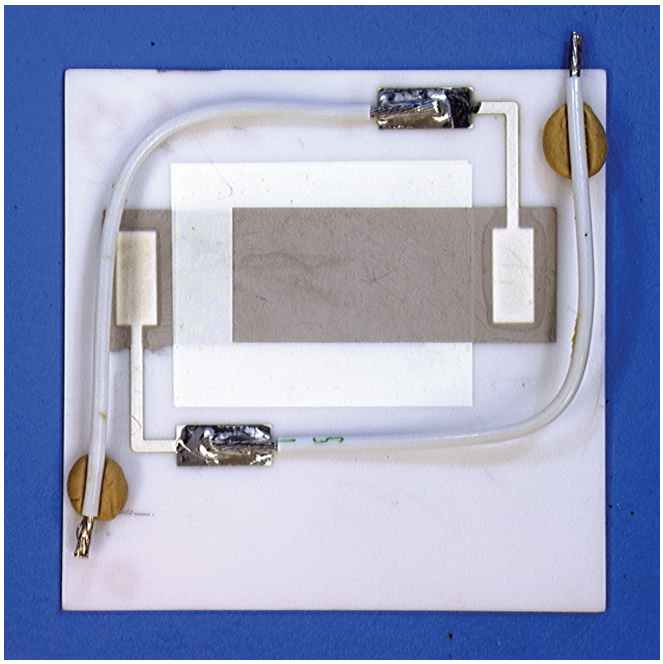

Figure 17. Ultracapacitor test cell made from SiO_2-coated $BaTiO_3$ deposited by screen printing.

Experiments were run to test for oxidation. A copper coupon and treated powders were sintered in the belt furnace. The copper became grey in color, which indicated that the copper had oxidized. Likewise, the treated powders also changed in color back to white. Measurements taken on the sintered powders (fig. 18) displayed a decrease in permittivity and DF, and an increase in ESR. The data trend indicates oxidation, and suggests that there was an oxygen leak inside the Nitrogen-purged belt furnace. This was undesirable, and adjustments were made to lower the oxygen parts per million.

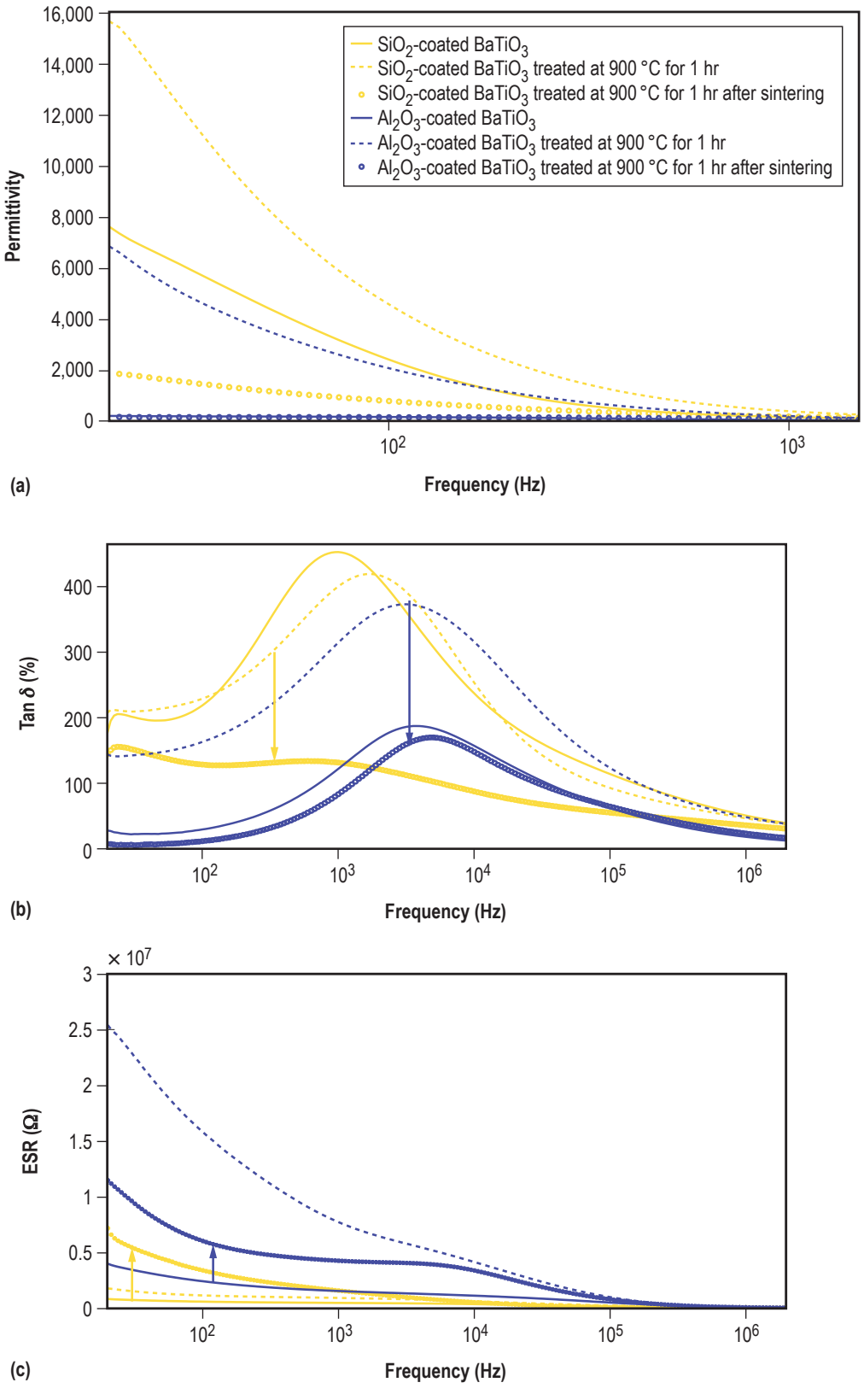

Figure 18. Plots of (a) permittivity, (b) DF, and (c) ESR powdered samples treated at 900 °C for 1 hr before and after furnace sintering.

SEM images (fig. 19) on the ultracapacitor test cells showed a 70% to 80% densification. The thickness for samples built using the 325 mesh was an average of 20 μm. Five out of 15 test cells had normal capacitor characteristics; the remaining (three SiO_2 and the rest Al_2O_3) were shorted.

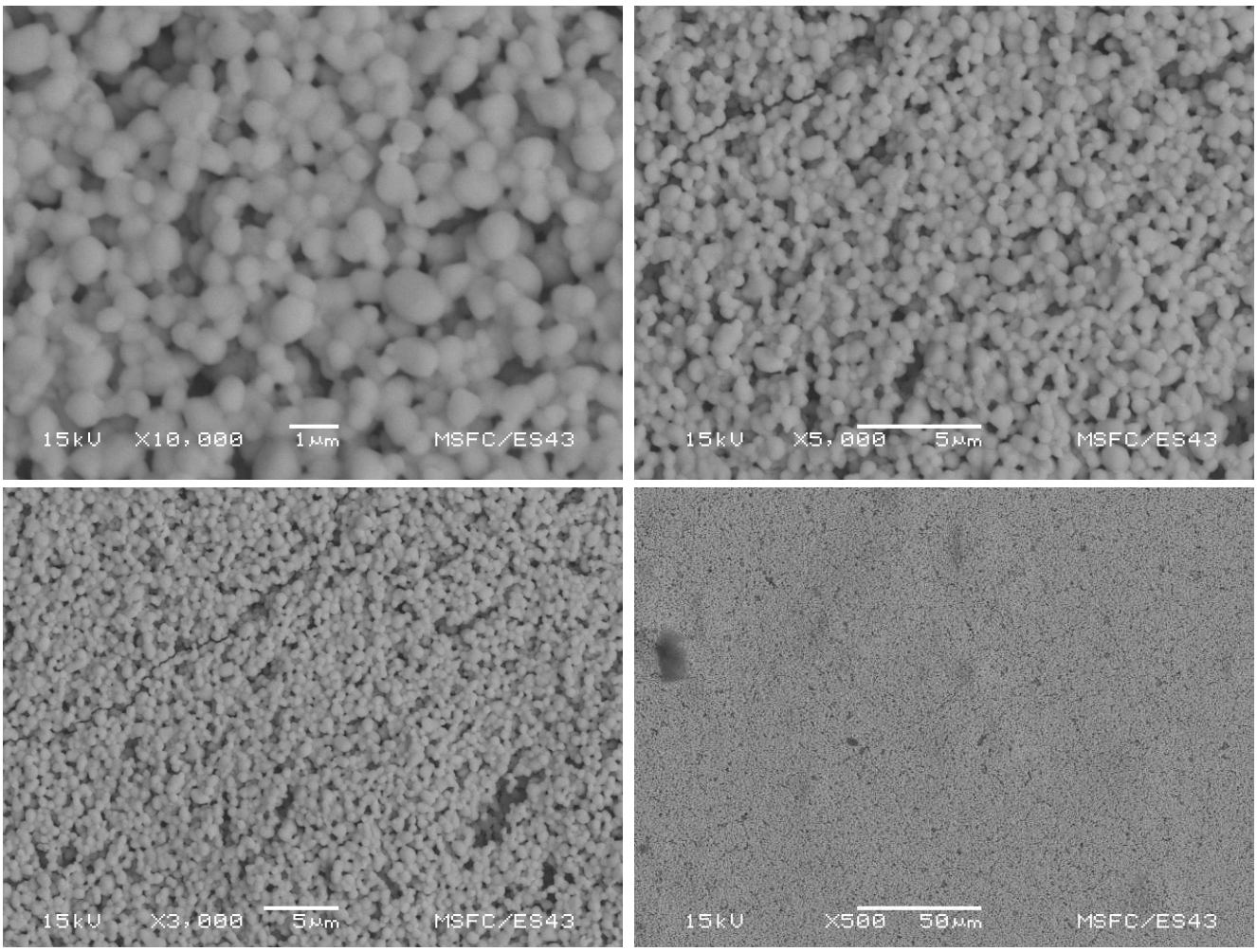

Figure 19. SEM image showing a 75% densification and the porosity of SiO_2-coated $BaTiO_3$ test cell with 184 nF of capacitance.

Table 7 shows the capacitor test cells built and their measured electrical characteristics. The thinnest capacitor was 13.5 µm. When tested at 50 V, the energy density was found to be 7.96×10^{-2} J/cc, and a capacitance of 125 nF at 1 kHz. The capacitance obtained through the discharge method using a DC source agrees with the capacitance values within ±5%. The voltage versus time plot for the 184.2 nF capacitor is shown in figure 20. If these devices can withstand 500 V, then one can expect 100× the energy storage, or about 8 J/cc. The voltage breakdown plot in figure 21 shows that some devices do withstand voltages exceeding 500 V.

Table 7. SiO_2-coated $BaTiO_3$ capacitor test cell characteristics.

Mesh	Capacitance (nF) at 1 kHz	Thickness (µm)	Electrode Area (mm^2)	Porosity (%)	Test Voltage (V)	Energy Density at Test Voltage (J/cc)
400	184.20	8.40	141.29	75	13	1.31×10^{-2}
400	73.34	111.90	146.32	70	25	0.14×10^{-2}
325	125.00	13.50	145.46	75	50	7.96×10^{-2}
325	125.00	24.73	141.24	75	25	1.12×10^{-2}
325	130.00	22.20	144.10	80	45	4.11×10^{-2}

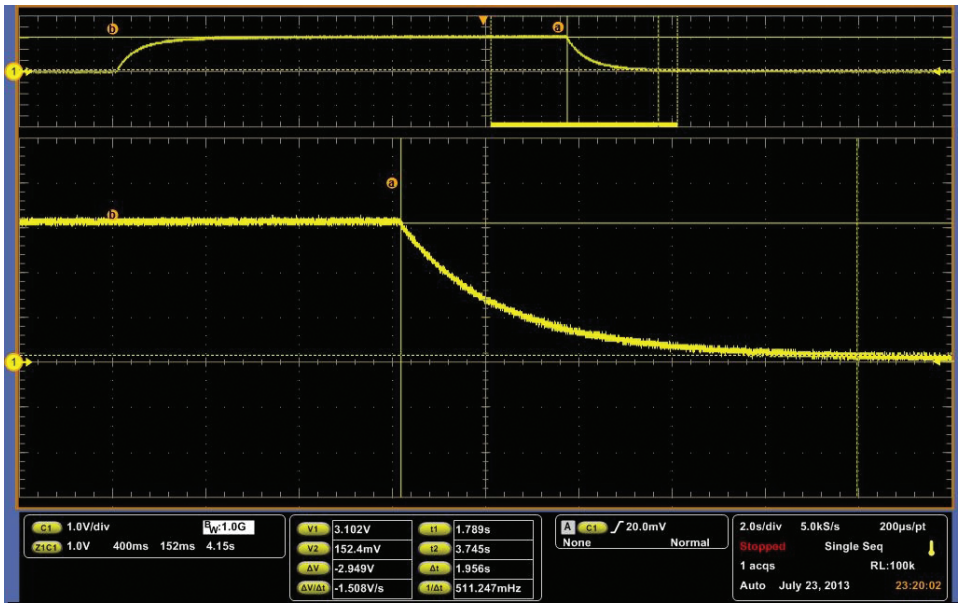

Figure 20. Voltage versus time plot used for the discharge method.

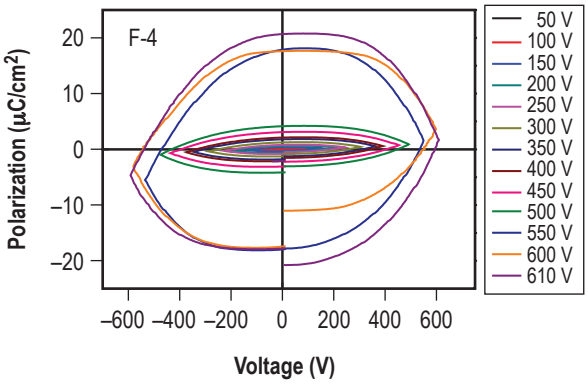

Figure 21. Breakdown curves for a device exhibiting breakdown >500 V.

Electrical characterization (fig. 22) shows normal capacitor behavior up to 1.3 MHz. Above the latter frequency, the capacitor test cells exhibit a negative capacitance and DF that spikes up to 3×10^3. This negative capacitance effect is observed in a variety of semiconductor devices.[20]

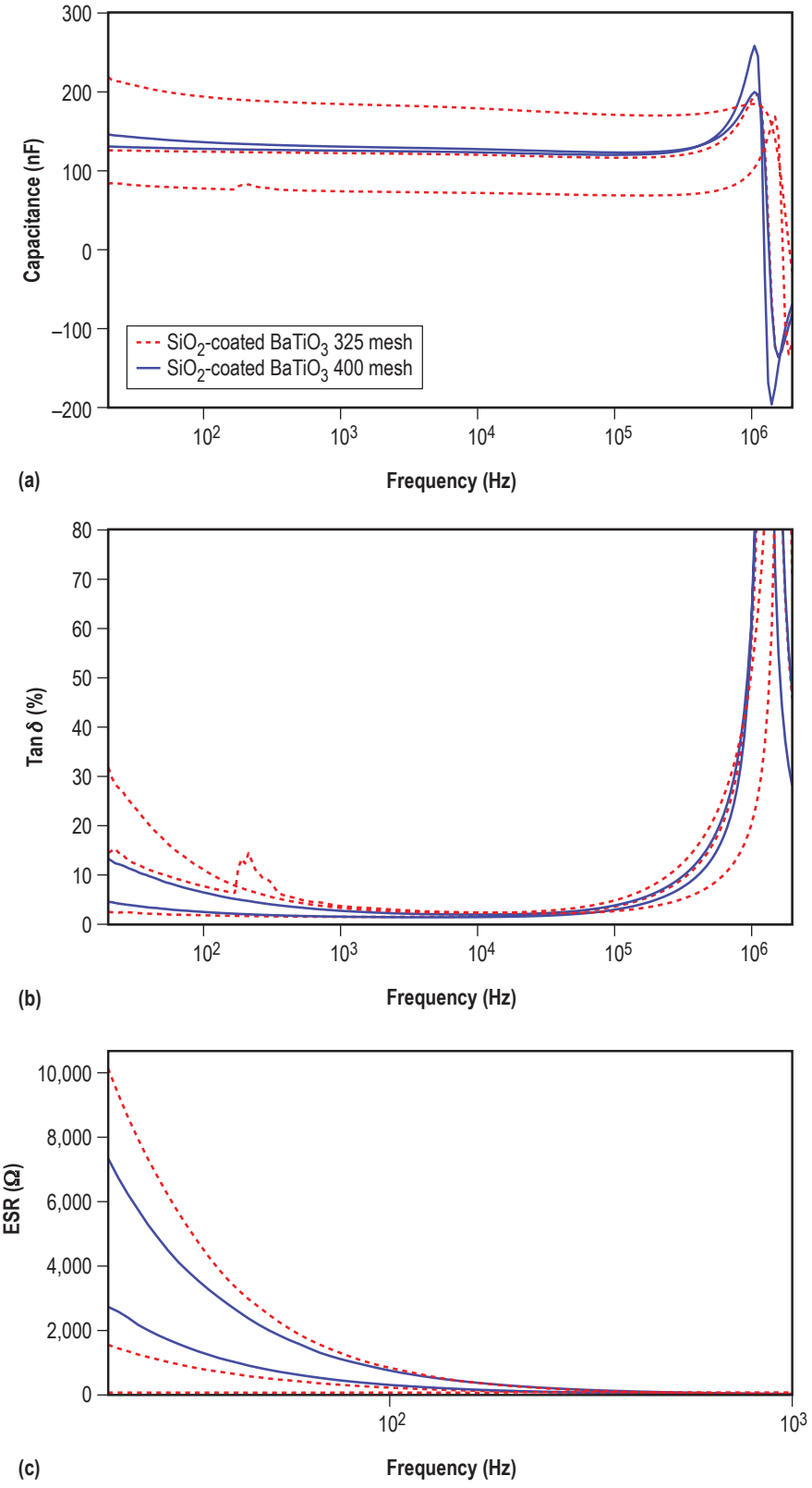

Figure 22. Plots of (a) capacitance, (b) DF, and (c) ESR capacitor test cells, made from the dielectric material treated at 900 °C for 1 hr before and after furnace sintering.

5. CONCLUSIONS

A material and set of processing conditions were selected that give the optimal properties for fabricating a device. The material of choice, SiO_2-coated $BaTiO_3$, exhibited the highest dielectric permittivity. This particular sample was treated at 900 °C for 1 hr. The processed material exhibited the following properties at 20 Hz: permittivity of 19,980, DF of 215%, and an ESR of 806 kΩ. A test cell was built with the selected material at a thickness of 13.5 μm, and it exhibited a capacitance of 125 nF at 1 kHz and an energy density of 7.96×10^{-2} J/cc at 50 V. The data indicate that the $BaTiO_3$, although properly reduced in the powder form, was subsequently oxidized due to an oxygen leak in the belt furnace when sintered in device form. Despite oxidizing the sample, the initial indications are that even in an oxidized state, the potential for large energy storage, especially at higher voltages, is possible.

Treatment at temperatures below 900 °C did not significantly affect the dielectric properties of the material. The decrease in properties for samples treated above 900 °C may be attributed to an overreduction or to excess interdiffusion. Though it did not experience a color change, SiO_2 obtained the highest initial and after-treatment permittivity. The color tone difference within a powder batch after being reduced indicates that a better sealed tube furnace or other synthesis techniques are necessary to obtain a homogeneous treatment.

The test cells' low densification (70%) must be improved. For better densification and characterization, a new technique will be developed. Densification can be increased while decreasing the thickness using other thin film deposition techniques such as aerosol jet deposition. For screen printing, a triple layer of dielectric material will be necessary to avoid shorted samples.

Finally, further study involving transmission electron microscopy and x-ray photoelectron spectroscopy are necessary to identify whether the ALD coating remains on the particles after synthesis and ink formulation, and to determine the role the coating plays in $BaTiO_3$ reduction. After ultracapacitor test cells are built, several of them will be connected in parallel (fig. 23), packaged (fig. 24), and tested for use in aerospace applications and common electronic devices.

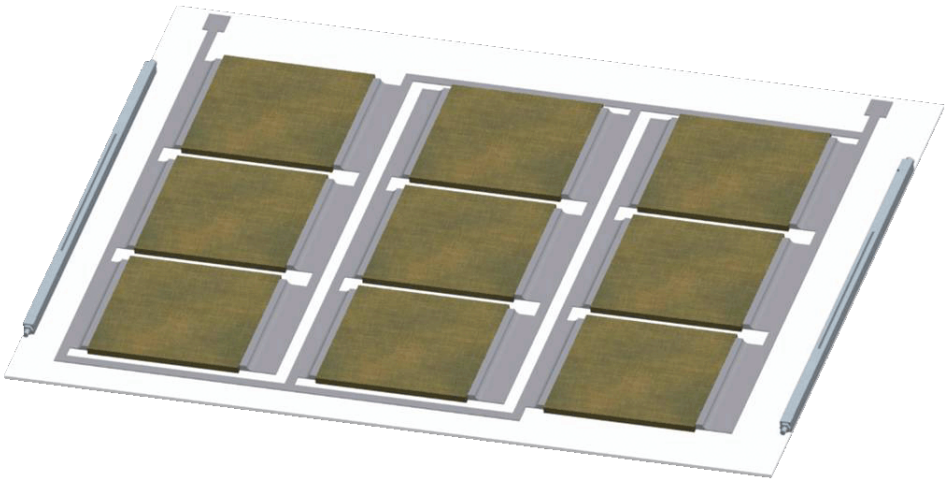

Figure 23. Ultracapacitor cells in parallel.

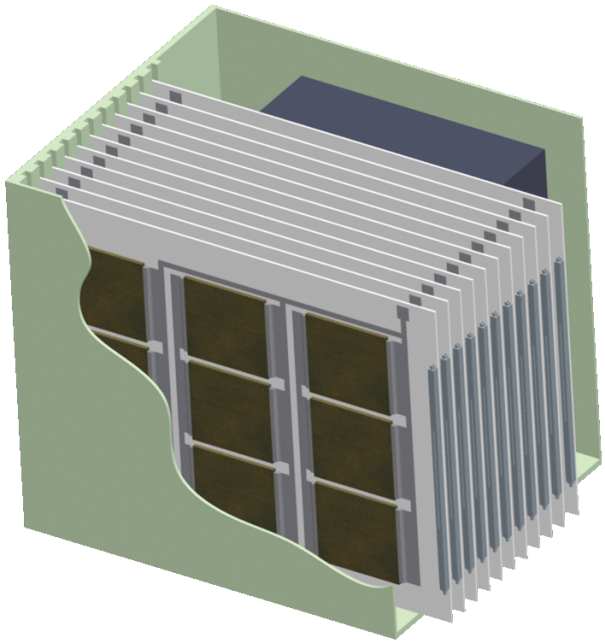

Figure 24. Ultracapacitor package.

REFERENCES

1. Chung, U.-C.; Elissalde, C.; Mornet, S.; et al.: "Controlling internal barrier in low loss $BaTiO_3$ supercapacitors," *Applied Physics Letters*, Vol. 94, No. 7, p. 072903, doi:10.1063/1.3076125, 2004.

2. Chen, Y.-C.: "Annealing effects of semiconducting barium-titanate thermister," *Journal of Marine Science and Technology*, Vol. 15, No. 4, pp. 307–314, 2007.

3. APC International, Ltd.: "BaTiO3 Specifications: Properties of Barium Titanate (BaTiO3)" <https://www.americanpiezo.com/single-crystals-non-pzt-materials/bati03-specifications.html>, 2013.

4. Guillemet-Fritsch, S.; Valdez-Nava, Z.; Tenailleau, C.; et al.: "Colossal Permittivity in Ultra-fine Grain Size $BaTiO_{3-x}$ and $Ba_{0.95}La_{0.05}TiO_{3-x}$ Materials," *Advanced Materials*, Vol. 20, No. 3, pp. 551–555, doi:10.1002/adma.200700245, 2008.

5. Halper, M.S.; and Ellenbogen, J.C.: "Supercapacitors: A Brief Overview," MP05W0000272, The Mitre Corporation, McLean, VA, 34 pp., March 2006.

6. National Instruments: "Capacitance/Inductance Measurements with PXI DMMs," <http://www.ni.com/white-paper/3078/en/>, February 3, 2017.

7. Wikipedia: "Electrical reactance," <http://en.wikipedia.org/wiki/Electrical_reactancance>, 2013.

8. Chu, A.; and Braatz, P.: "Comparison of commercial supercapacitors and high-power lithium-ion batteries for power-assist applications in hybrid electric vehicles: I. Initial characterization," *Journal of Power Sources*, Vol. 112, No. 1, pp. 236–246, October 2002.

9. Wikipedia: "Equivalent series resistance," <http://en.wikipedia.org/wiki/Equivalent_series_resistance>, 2013.

10. Fiore, R.: "ESR Losses In Ceramic Capacitors," ATC 001-923 Rev. D; American Technical Ceramics, <www.atceramics.com/documents/notes/esrlosses_appnote.pdf>, 2013.

11. Wikipedia: "Dissipation factor," <http://en.wikipedia.org/wiki/Dissipation_factor>, 2013.

12. Kötz, R.; and Carlen, M.: "Principles and applications of electrochemical capacitors." *Electrochimica Acta*, Vol. 45, Nos. 15–16, pp. 2483–2498, May 2000.

13. Artemenko, A.; Elissalde, C.; Chung, U.-C.; et al.: "Linking hopping conductivity to giant dielectric permittivity in oxides," *Applied Physics Letters*, Vol. 97, No. 13, p. 132,901, doi:10.1063/1.3495779, 2007.

14. Mornet, S.; Elissalde, C.; Hornebecq, V.; et al.: "Controlled growth of Silica Shell on $Ba_{0.6}Sr_{0.4}TiO_3$ Nanoparticles Used as Precursors of Ferroelectric Composites," *Chemistry of Materials*, Vol. 17, No.17, pp. 4530–4536.

15. Ishii, Tatsuya; Endo, M.; Masuda, K.; and Ishida, K.: "The possibility of giant dielectric materials for multilayer ceramic capacitors," *Applied Physics Letters*, Vol. 102, No. 6–062901, 2013.

16. Hennings, D.F.K.: "Dielectric materials for sintering in reducing atmospheres," *Journal of the European Ceramic Society*, Vol. 21, Nos. 10–11, pp. 1637–1642, 2001.

17. Buessem, W.R.; and Marshall, P.A.: *Crystal Chemistry of Ceramic Dielectrics*, Linden Labs, Inc., State College, PA, 1963.

18. Saburi, O.: "Properties of semiconductive barium titanates," *Journal of the Physical Society of Japan*, Vol. 14, No. 9, pp. 1159–1174, 1954.

19. Goswami, A.K.: "Dielectric Properties of Unsintered Barium Titanate," *Journal of Applied Physics*, Vol. 40, No. 2, pp. 619–624, 1969.

20. Ershov, M.; Liu, H.C.; Buchanan, M.; et al.: "Negative capacitance effect in semiconductor devices," *IEEE Transactions on Electron Devices*, Vol. 45, No. 10, pp. 2196–2206, doi:10.1109/16.725254, 1998.

REPORT DOCUMENTATION PAGE

Form Approved
OMB No. 0704-0188

1. REPORT DATE *(DD-MM-YYYY)*	2. REPORT TYPE	3. DATES COVERED *(From - To)*
01–08–2017	Technical Memorandum	

4. TITLE AND SUBTITLE

A Novel Solid State Ultracapacitor

5a. CONTRACT NUMBER

5b. GRANT NUMBER

5c. PROGRAM ELEMENT NUMBER

6. AUTHOR(S)

A.Y. Cortés-Peña*, T.D. Rolin, S.M. Strickland, and C.W. Hill**

5d. PROJECT NUMBER

5e. TASK NUMBER

5f. WORK UNIT NUMBER

7. PERFORMING ORGANIZATION NAME(S) AND ADDRESS(ES)

George C. Marshall Space Flight Center
Huntsville, AL 35812

8. PERFORMING ORGANIZATION REPORT NUMBER

M–1438

9. SPONSORING/MONITORING AGENCY NAME(S) AND ADDRESS(ES)

National Aeronautics and Space Administration
Washington, DC 20546–0001

10. SPONSORING/MONITOR'S ACRONYM(S)

NASA

11. SPONSORING/MONITORING REPORT NUMBER

NASA/TM—2017–219686

12. DISTRIBUTION/AVAILABILITY STATEMENT

Unclassified-Unlimited
Subject Category 44
Availability: NASA STI Information Desk (757–864–9658)

13. SUPPLEMENTARY NOTES

Prepared by Space Systems Department, Engineering Directorate
*Johnson Space Center, Houston, TX; **CK Technologies, Meridianville, AL

14. ABSTRACT

Novel dielectric materials were researched to develop an internal barrier layer capacitor that is fully solid state. These materials included reduced nanoparticles of barium titanate that were coated with various atomic layer deposited oxides. The nanoparticle powders were then densified into pellets and characterized using a dielectric test fixture over a frequency range of 20 Hz to 2 MHz. Densification and sintering were evaluated using scanning electron microscopic techniques. Ultimately, the samples showing the most promising electrical characteristics of permittivity, dissipation factor and equivalent series resistance were chosen to manufacture devices for subsequent testing.

15. SUBJECT TERMS

battery, capacitor, ultracapacitor, supercapacitor, electrical, electronic, electromechanical parts, barium titanate, additive manufacturing, nanomaterials, energy storage

16. SECURITY CLASSIFICATION OF:			17. LIMITATION OF ABSTRACT	18. NUMBER OF PAGES	19a. NAME OF RESPONSIBLE PERSON
a. REPORT	b. ABSTRACT	c. THIS PAGE			STI Help Desk at email: help@sti.nasa.gov
U	U	U	UU	44	19b. TELEPHONE NUMBER *(Include area code)* STI Help Desk at: 757–864–9658

National Aeronautics and
Space Administration
IS02
George C. Marshall Space Flight Center
Huntsville, Alabama 35812